High-resolution integral-field spectroscopy of exoplanets
Haffert, S.Y.

Citation
Haffert, S. Y. (2019, November 26). *High-resolution integral-field spectroscopy of exoplanets*. Retrieved from https://hdl.handle.net/1887/80839

Cover Page

Universiteit Leiden

Author: Haffert, S.Y.
Title: High-resolution integral-field spectroscopy of exoplanets
Issue Date: 2019-11-26

1 | Introduction

Almost three decades ago our perception of the universe changed drastically. The first planet around a star other than our own Sun had been found (Wolszczan & Frail, 1992). This system was and still is rather unique because the two planets are orbiting a pulsar, the remnant of a star after it has created a supernova. This fact puzzled astronomers because there were no known methods at that time for planets to survive a supernova. Another possibility was that they formed from the left-over debris (Rasio et al., 1992; Tavani & Brookshaw, 1992). The second shock came when the first exoplanet orbiting a solar-like star was discovered just three years later (Mayor & Queloz, 1995). The planet, 51 Pegasi b, is in a very short-period orbit of only 4.23 days and roughly half the mass of Jupiter. It was very surprising to find a planet comparable to Jupiter orbiting their host star much closer than that Mercury is orbiting around the Sun. More Jupiter-like planets on close-in orbits followed soon (Butler et al., 1997; Marcy & Butler, 1996). This class of gas-giant planets was quickly termed 'hot Jupiters' because the close proximity to their host star leads to high equilibrium temperatures.

In the years after these first few discoveries the field of exoplanet research quickly expanded. Many observing techniques and instruments were developed, leading to an explosive growth in the number of discovered planets, which can be seen in Figure 1.1. Most exoplanets to date have been found by the Kepler mission, which added almost 2500 planets. The Kepler mission used the transit method where stars are closely monitored to search for periodic dimmings when the planet moves in front of the star (Borucki et al., 2010; Henry et al., 2000). Kepler revealed that there are many exotic planets and planetary systems. A surprising find was the detection of many super-Earths and sub-Neptunes with masses of a few times that of the Earth (Petigura et al., 2013a,b). These types of planets are the most ubiquitous in the Milky Way even though our own Solar system does not have any of them (Petigura et al., 2013a,b).

Next to super Earths there are also less common but stranger planets like Kepler 51 b and d that have densities similar to cotton candy (Masuda, 2014) or the extremely hot KELT-9b that has gaseous iron and titanium in its atmosphere (Gaudi et al., 2017; Hoeijmakers et al., 2018b). Not only is there a large diversity in the planets themselves but there is also a large diversity in the composition of planetary systems: Trappist-1 has seven Earth-mass planets with short orbital periods around an M-dwarf star (Gillon et al., 2017), but HR8799 has four giant gas planets on very wide orbits (Marois et al., 2008, 2010).
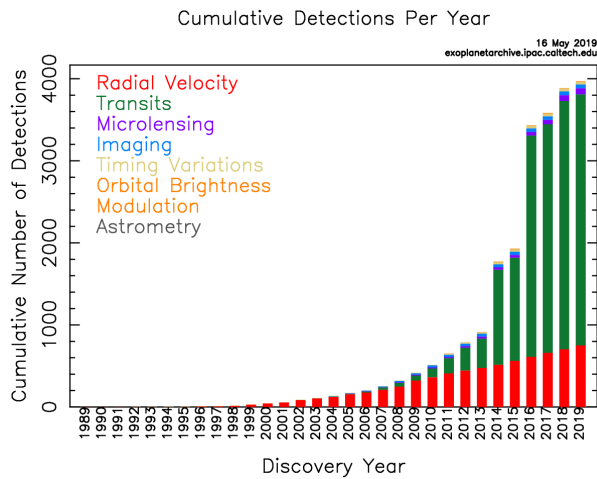
Figure 1.1: The amount of planets discovered by different observational techniques as a function of time. The number of planets found through radial velocity has been roughly linearly increasing with time. The amount of planets found by the transit method has exploded with obvious jumps in 2014 and 2017. In those years Kepler data were released, which shows the major impact Kepler had in the field of exoplanets. Other techniques are lagging behind in the number of detections. This graph was create with the NASA exoplanet archive on 16 May 2019.

This variety in exoplanets and planetary systems is challenging the theories of planet formation because the entire range of observed planetary-system architectures must be explained. The initial conditions for planet formation are set by the formation of the host star. Therefore the formation of planets cannot be understood independently from star formation. Stars are formed from clouds of molecular gas in the interstellar medium. Small overdensities in these large, cold clouds can create gravitational instabilities thath lead to the local collapse of the gas clouds into proto-stellar cores (McKee & Ostriker, 2007). If the collapsing gas has some angular momentum, it will flatten out the collapsing cloud and form a disk with the proto-star at its center. The surrounding dust and gas will gather into the circumstellar disk, which is thought to be the birth place of planets and is therefore also called a protoplanetary disk (Armitage & Belmonte, 2018). There are several proposed mechanism through which planets can form, and they broadly fall into one of the following three categories:

1. The planet forms through core accretion where small dust particles slowly coagulate into a proto-planetary core (Pollack et al., 1996). As the core grows, its gravity also grows, and it will attract more dust. When the proto-planet is massive enough it will start to rapidly accrete the gas and dust in its surrounding, thereby clearing out a path in the circumstellar disk through runaway accretion. This process stops when the proto-star becomes luminous enough to clear the disk through radiative pressure.

2. There are several mechanism through which the protoplanetary disk can become unstable and fragment into self-gravitating clumps. The most common method proposed for this are gravitational instabilities Boss (1997) that are created if the disk is very massive. But recent ALMA observations have revealed that massive disks are not very common, and this makes the gravitational instability process possibly a very rare event (Andrews et al., 2013; Pascucci et al., 2016). In the last few years it has been argued that magneto-rotational instabilities (MRI) may also cause disk fragmentation that leads to planet formation (Chiang & Youdin, 2010).

3. During the collapse of the pre-stellar core the clump of gas and dust can break up into separate clumps (Hennebelle & Chabrier, 2008). The separated clumps then can continue to contract and form planets. This scenario is very similar to the formation of binary star systems albeit with a more extreme mass ratio.

It is possible that all three processes play a part in the formation of planets. One of the challenges will be to determine which process dominates the formation process for which class of planets. It has been suggested that gas giants onwide orbits like those in the HR8799 system have been formed through gravitational instability (Nero & Bjorkman, 2009). However there is also contradicting evidence that their masses and separation do not fulfill several of the criteria for the formation through such instabilities (Bowler et al., 2015; Rameau et al., 2013; Vorobyov, 2013).

The interaction between the planet and the protoplanetary disk is thought to be quite complex (Kley, 2017). The planet can change its orbital distance, either moving in or out, due to planet-disk interaction. The more massive planets are able to sweep up a major part of the disk material in their orbit and carve a deep gap in the disk. The depletion of the dust and gas in the disk changes the pressure gradient and forces the planet to migrate; this migration scenario is called type-I migration (Kley, 2017; Nelson et al., 2000). Planets of a few Earth masses follow a different migration scenario called type II (Nelson et al., 2000) where only a small shallow gap is created that is not completely cleared of dust and gas. The main difference between the different types is the amount of matter that is accreted, and that determines whether the planet-disk interaction is linear (type II) or non-linear (type I). The case for multiple planets is more complicated since the planets will also influence each other, which is classified as type-III migration. In the past decades complex hydro-dynamical simulations have been conducted to understand the behaviour of migrating planets, leading to the development of semi-analytical relations between the migration rate, disk parameters and planet parameters (Dodson-Robinson & Salyk, 2011; Kley, 2017).

Theories of planet formation are currently tested by incorporating these semi-analytical relations, such as those for planetary migration, in a single global simulation environment (Benz et al., 2014; Mulders et al., 2018). Such codes try to replicate the observed exoplanet populations and are therefore called planet-population synthesis codes. Both the transit method and the radial velocity method mostly reveal old planetary systems because young stars produce a large quantity of astrophysical noise due to e.g. star spots or circumstellar material (Crockett et al., 2012; Lee, 2017; van Eyken et al., 2012; Yu et al., 2015). Therefore we can only compare the end state of the population synthesis codes and tweak the parameters until the simulations match the observed statistics. While this already has provided significant information about planet formation, we still have not verified

most of the physical mechanisms in these population codes (Morbidelli &
Raymond, 2016).

Direct imaging plays an important role to overcome these observational
limitations. By spatially resolving the disk and the embedded planets, we
can witness their interaction. Another added benefit is the enhanced in-
trinsic contrast between the star and the planets. For old systems such
as our own solar system, the best signal we could use to detect Earth or
Jupiter from a distance is through reflected light. The intensity ratio be-
tween the Sun and the reflected light of Earth and Jupiter are 10^{-10} and
10^{-9}, respectively (Traub & Oppenheimer, 2010). This is a huge contrast
to overcome. But during the first stages of planet formation, the planets
are still very hot. This increases the intrinsic contrast in the Near-Infrared
to $10^{-5} - 10^{-6}$ (Burrows et al., 2004) making the detection of such exo-
planets orders of magnitude easier. This shows that direct imaging is the
prime technique to observe young planetary systems and their planet-disk
interactions.

1.1   The direct imaging challenge

1.1.1   The Earth atmosphere

Direct imaging of exoplanets is a challenging task because a high contrast
needs to be reached at very close angular separations. If we place our
solar system at 100 parsec, the resolving power necessary to separate Earth
from the Sun would need to be better than 10 milliarcseconds (mas), but
even if we could resolve Earth, the contrast between the Earth and the
Sun of about 10^{-10} will make Earth close to impossible to observe. For
Jupiter it becomes slightly easier with a separation of 55 mas and a contrast
of $10^{-8} - 10^{-9}$. To resolve Earth and Jupiter at this distance we would
need to use large telescopes of at least 30 meters in diameter, under the
assumption that we will be able to solve the contrast-ratio problem. This
angular resolving power will become available in the next decade with the
construction of the upcoming extremely large telescopes; the Extremely
Large Telescope (ELT) spearheaded by ESO, the Thirty Meter Telescope
(TMT) and the Giant Magellan Telescope (GMT). But until those are
build, we will have to use the current 8 and 10-meter class telescopes that
are limited to about 26 mas angular resolution at 1 μm by diffraction,

$$\Delta\theta = 1.22\lambda/D. \qquad (1.1)$$

Here $\Delta\theta$ is the angular resolving power, λ the wavelength that is used for imaging and D the telescope diameter. While the current generation of telescopes like the Very Large Telescope (VLT) of ESO, with an 8.2-meter diameter, would be able to resolve Jupiter at 100 pc, we have not been able to do this. For ground-based telescopes there are two challenges to overcome. The first being turbulence in the Earth's atmosphere, and the second is the intrinsic contrast between the planet and its host star. When light propagates from a star towards the Earth, it becomes a smooth plane wave due to the large distance between us and the star. It travels over several years to tens or hundreds of year,s and when it finally reaches Earth the light has to travel through the atmosphere to enter our telescopes. During the last tenth of a milliseconds of its journey the light wave loses its flatness because of turbulence in the atmosphere (Fried, 1966). This turbulence will create wavefront aberrations that degrade the resolving power of the telescope. The amount of wavefront aberration depends on the turbulence strength that is parametrised by the Fried parameter r_0 (Fried, 1966). The Fried parameter is the characteristic spatial scale of the perturbed wavefront where the wavefront changes by less than one radian. The resolution limit of the telescope is set by this characteristic scale instead of the telescope diameter. In median weather conditions the Fried parameter is roughly 20 to 30 cm at 1 μm for good observing sites such as Paranal, La Palma or Mauna Kea. The resolution that the VLT achieves during these condition is about 1 arcsecond, almost 40 times larger than the diffraction limit! This can be seen in Figure 1.2.

1.1.2   Adaptive optics

Almost 70 years ago Horace Babcock proposed the idea of adaptive optics to remove the effects of atmospheric turbulence (Babcock, 1953). A simple sketch of an adaptive optics (AO) system is shown in Figure 1.3. Every AO system contains an adaptive element that can change its shape in such a way that it compensates for the wavefront distortions caused by the atmosphere. Usually a deformable mirror (DM) is used because of its achromatic response. After reflecting of the DM surface, the wavefront has become flat again, and the telescope can reach its diffraction limit. The operation of such an AO system is complex, and several sub-systems are necessary. The most important sub-system is the wavefront sensor (WFS). Detectors in the visible and near-infrared can only measure the intensity of the light and not its phase. Therefore a specialized piece of optic, the wavefront sensor, is necessary to change the wavefront errors into intensity
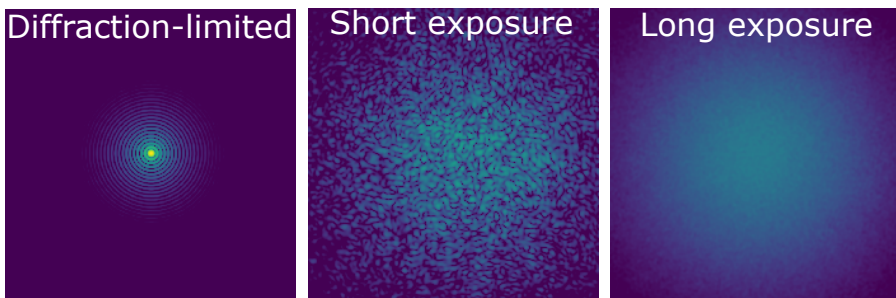
Figure 1.2: The effects of turbulence are shown here for an 8-meter class telescope with a seeing of 1 arcsecond. The left image shows the theoretical diffraction pattern for a circular telescope. In the centre an image is shown of a very short integration time effectively freezing the atmosphere during that time frame. The effects of turbulence are very apparent in this image, the Point-Spread-Function(PSF) is broken up into many individual speckles. A long integration where the PSF is averaged over many realizations of turbulence can be seen on the right. This seeing-limited PSF is smeared out over a large area reducing the resolving power.
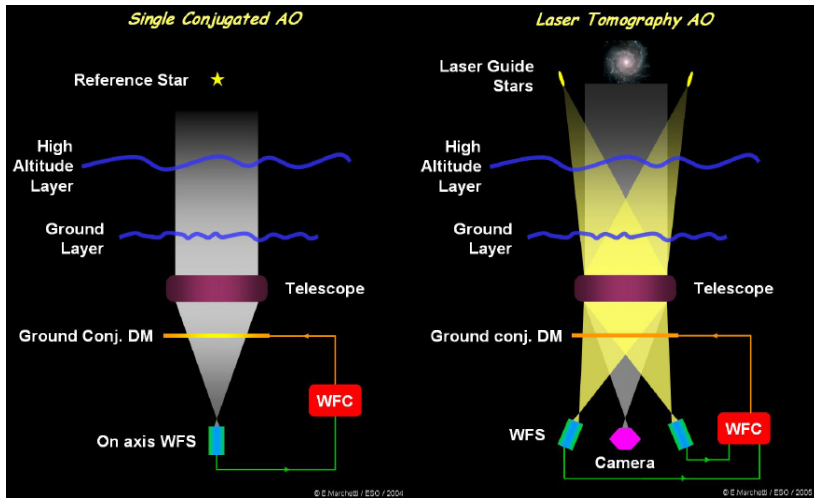
Figure 1.3:   These two figures show different types of adaptive optics. The left uses the light from the astrophysical target itself to do wavefront sensing, while the right scheme uses an artificial light source created by a powerful laser that is reflected by the upper atmosphere. Both methods drive a single deformable mirror to correct for the wavefront aberrations. Image credit: ESO.

modulations on the detector. The standard AO system as drawn in Figure 1.3 uses a WFS to measure wavefront deviations and feeds those back to the DM to create a closed-loop feedback system. The AO system needs to operate at several hunderd Hz to several thousand Hz because of the time scale over which the atmosphere changes (Greenwood, 1977). The coherence time of the atmosphere τ_0 is roughly r_0, the Fried parameter, divided by the wind speed v (Greenwood, 1977). This leads to a coherence time on the order of 1 ms to 10 ms, which is why AO systems need to do the corrections in real time.

The AO system that has been described here is a so called Single-Conjungate Adaptive Optics (SCAO) system. In a SCAO system there is one DM that is used for on-axis correction of the turbulence, and the light of the target itself is used for wavefront sensing. The first generation of AO instruments, NACO at the VLT (Lenzen et al., 2003; Rousset et al., 2003) and NIRC2 at KECK (Wizinowich et al., 2000), began their operations in the early 2000's. They all used the SCAO configuration because it is

relatively easy to implement and has the potential to provide the highest possible on-axis correction. Many astronomers used these early AO instruments for direct imaging while they had not been specifically developed for exoplanet science (Chauvin et al., 2005). The potential of AO instruments for direct imaging was proven by the detection of multiple planets around HR8799 (Marois et al., 2008, 2010). This system came as a surprise because most planets found until then were much closer to their host star, making HR8799 a still unique planetary system.

SCAO has worked very well for the purpose of improving the image quality but it is limited to bright targets because the light from the star itself is used to measure the wavefront errors created by the atmosphere. In the past two decades a large amount of work has been done to make AO-corrected images accessible for fainter targets. Instead of using the light from the astrophysical object an artificial light source is generated with a powerful laser high up in the atmosphere (Foy & Labeyrie, 1985; Fugate et al., 1991). For large telescopes a sodium laser is used to excite atoms in the sodium layer of Earth's atmosphere (Bonaccini Calia et al., 2010). The excited atoms will become an articial light beacon that can be used to measure the atmospheric turbulence. Due to the brightness of the laser it is not possible to bring the laser close to the astrophysical source, it needs to be pointed slightly away from the target. The atmospheric volume that is probed by this laser is slightly different than the volume that the star passes through. This led to the development of Laser Tomography Adaptive Optics (LTAO) where multiple laser guide-stars are placed around the target of interest (Hubin et al., 2005; Tallon & Foy, 1990). The measurements from the different lasers are then combined to create the best estimate of the on-axis wavefront errors. ESO applied this in the Adaptive Optics Facility (AOF) for the VLT that saw first light in 2015 (Madec et al., 2018). It has since then produced spectacular images, see for example Fig 1.4.

1.1.3   High-contrast imaging

The first generation of dedicated planet-hunting instruments SPHERE (Beuzit et al., 2019), GPI (Macintosh et al., 2014) and SCEXAO (Jovanovic et al., 2015) saw first light in 2013 and 2014. These instruments incorporated major instrumental advances to improve the performance for the detection and characterization of exoplanets. The AO systems contain DMs that have many more degrees of freedom operating above 1 kHz as opposed to the few hundred Hz of instruments such as NACO. These improvements allow for almost perfect correction and are therefore termed as Extreme Adaptive

Figure 1.4:   Observations of Neptune with the new Narrow Field Mode of MUSE with AO correction provided by the LTAO system. The LTAO shows almost diffraction-limited performance. Image credits to ESO/P. Weilbacher (AIP).

Optics (XAO). With the current generation of high-contrast imagers (HCI) we can reach diffraction-limited performance in the near-infrared. But this is not enough to find faint planets as the planet is still much fainter than the Airy rings of the stellar diffraction pattern. With the high quality of the PSFs of SPHERE and GPI they can also use advanced coronagraphs to remove the diffraction effects of the star.

A coronagraph is a specialized optical device that is designed as an extreme angular filter; the on-axis starlight needs to be suppressed as much as possible while leaving the off-axis planet light unaltered. One of the first coronagraphs to be used for exoplanet imaging was the classical Lyot coronagraph, originally developed to observe the solar corona outside of a total solar eclipse (Lyot, 1939): an opaque disk with a size of a few λ/D is added in the focal plane. This mask blocks part of the light, but due to the hard edges of the mask, some of the on-axis light still diffracts around it. Because the edge of the mask is much smaller than λ/D, this diffracted light will scatter outside of the geometric pupil, which can then be blocked by placing an additional aperture mask, the Lyot stop, in a pupil after the focal-plane mas. The classical Lyot coronagraph reduces the starlight by several orders of magnitude. More advanced focal-plane

masks have been developed that theoretically can remove all starlight if the input wavefront has no aberrations (Foo et al., 2005; Guyon, 2003; Rouan et al., 2000; Soummer, 2005). Another class of coronagraphs called pupil plane coronagraphs place masks in the pupil of the telescope to modify the shape of the PSF. By manipulating the amplitude or phase in the pupil, the electric field in the focal plane can be made to destructively interfere. With this technique dark holes can be created where we can search for planets, and because the optics are in the pupil, they are insensitive to vibrations. There are currently two flavours of pupil-plane coronagraphs, the Shaped Pupil (SP) coronagraph that uses amplitude masks (Kasdin et al., 2003; Soummer et al., 2003) and the Apodizing Phase Plate (APP) coronagraph that uses phase plates (Codona et al., 2006; Otten et al., 2017; Snik et al., 2012).

For Lyot-style coronagraphs the PSF needs to be perfectly aligned with the focal plane mask to cancel the starlight, but due to vibrations and small drifts the star will not be perfectly aligned with the mask. This deteriorates the performance of the coronagraph (Ruane et al., 2017). Pupil-plane coronagraphs are less sensitive to theses issues because the optical elements are in the pupil. Next to vibrations all other wavefront errors will also degrade the performance of the coronagraph (Aime & Soummer, 2004). There are still residual wavefront errors even though an AO system is used. The residual wavefront errors have two sources, the first being residual wavefront errors from the atmosphere that are not correctable or not completely removed. The second is due to a difference in the optical path between the coronagraphic optics and the wavefront-sensor optics. Because these instruments have different optics, they will see a slightly different wavefront error causing differential wavefront errors between the two systems. These wavefront errors are called Non-Common Path Aberrations (NCPAs). A lot of current research is focused on mitigating these NCPAs (Jovanovic et al., 2018). Both the NCPAs and the residual turbulence causes speckles that can look like planets. Image-processing algorithms are used to further remove these speckles.

1.1.4   Post-processing

To further enhance the contrast, advanced post-processing algorithms are used to minimize the starlight while leaving the planet light unaltered as much as possible. These techniques aim to model the PSF and speckle field of the star, which can then be subtracted from the image to reveal the planet. The most straightforward technique is to observe a reference

object and then subtract its PSF from the science target. Because this reference object is used to measure the PSF, it should not include any circumstellar material or companions. This technique is called Reference Differential Imaging (RDI) and was one of the first HCI techniques and was able to reveal the circumstellar disk around Beta Pictoris (Smith & Terrile, 1984). RDI has also been very successfully applied to Hubble Space Telescope (HST) data because HST has a very stable PSF (Schneider & Silverstone, 2003). If it is not possible to use a reference target, either due to unavailability or because the speckle pattern is not repeatable for different targets, a PSF model has to be built from the data itself. To create the reference PSF in this case, one needs to make use of a difference between the star and the planet.

The most successful method is based on angular rotation. The contributions from the star and planet can be separated when the field rotates but the pupil is stable because the star is on-axis and the planet is off-axis. During the rotation the PSF of the star will stay fixed in the image while the planet will rotate. The planet signal will therefore have a different temporal behaviour from the static speckles. The different observations are median combined, and because the planet is at different positions for every observation, it will not affect the median. The median-combined data are then a good model for the PSF. After subtracting the PSF model the data is derotated and combined to create the final image that can reveal faint point sources. This technique is called Angular Differential Imaging(ADI) and has been the most successful differential imaging technique for the detection of giant planets (Marois et al., 2006). ADI is quite a natural way of observing with an alt-azimuth telescope where the field will rotate due to the rotation of the Earth. Space-based telescopes usually employ different roll angles to rotate the image (Schneider & Silverstone, 2003). RDI and ADI require stable PSFs and speckle patterns, and depending on the speckle statistics either ADI or RDI reaches deeper constrast levels (Ruane et al., 2019). If the the speckle patterns change between observations, they will not be removed, and the achievable contrast limit is set by the speckle-noise limit (Aime & Soummer, 2004; Martinez et al., 2013). This is not an issue far away from the star as the speckles average out quite well, and the speckle noise limit is usually below the photon noise limits. But close to the star the speckles change slowly, and the photon-noise limit is many times higher due to the brightness of the Airy rings (Racine et al., 1999). Both RDI and ADI are therefore limited in power close to the diffraction limit. The effects of slowly evolving speckles can be seen in Figure 1.5
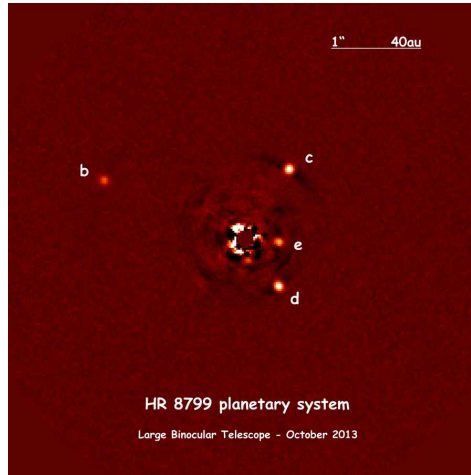
Figure 1.5:   An observation of the HR8799 system taken with the LBT
(Maire et al., 2015) and post-processed with Angular Differential Imag-
ing. The four planets orbiting the star are clearly resolved. Searching for
planets closer in is difficult due to slowly changing speckles that limit how
close in we can search. The speckle noise can be seen at the edge of the
coronagraphic mask were the intensity quickly changes from white to black.

where limited improvement is achieved close to the star. Diversities that
are based on the intrinsic properties of the observed system that are time
invariant would be more robust against these varying speckles.

1.1.5   The powers of ten in exoplanet spectroscopy

Evolutionary models of exoplanets predicted a strong methane signal sim-
ilar to field brown dwarfs (Baraffe et al., 2003). Simultaneous Differential
Imaging takes advantage of this difference by observing in two narrowband
filters (Marois et al., 2005; Racine et al., 1999). One narrowband filter
targeting the methane absorption band at 1.62 μm and one just outside of
the band to measure the continuum. The difference between the two ob-
servations should reveal the planet. Although SDI in the methane feature
looked like a promising technique, it has not been fruitful (Biller et al.,
2007). Recent work shows that planets typically do not contain strong
methane absorption features (Konopacky et al., 2013; Petit dit de la Roche
et al., 2018; Skemer et al., 2014). A feature that is promising and has shown
success is the emission of hydrogen. Hα emission is one of the strongest

signposts of a planet in formation (Aoyama et al., 2018; Marleau et al., 2017; Zhu, 2015), which occurs when gas is deposited onto the planet at high velocity. As the gas collides with the planet, it creates a strong shock front, which heats up the local gas to high temperatures (T>10000 K). This process generates a large amount of Hα emission, which decreases the contrast between the star and planet by several orders of magnitude, thereby making it easier to detect. The difference between two narrowband filters with one covering Hα and the other in the nearby continuum can be used to subtract out the star (Close et al., 2014).

A higher-resolution version of this is Spectral Differential Imaging, (having the same abbreviation as Simultaneous Differential Imaging). With SDI the PSF is measured at many wavelengths, usually with a low-resolution integral-field spectrograph at a resolving power of $R = 50-100$ over a large bandwidth. Due to the properties of diffraction the PSF and its speckles scale radially with wavelength while the planet stays at a fixed position (Sparks & Ford, 2002; Thatte et al., 2007). Rescaling the data to a reference wavelength will overlay the speckles while smearing out the planet. Taking a median as is done with ADI will create a PSF model that can be used for subtraction. Some planet signal is also subtracted by this procedure; the amount of planet subtraction depends on the observed bandwidth and the angular distance of the planet. SDI has the advantage that it can remove the starlight and at the same time characterize the planet at low resolving power. This is very powerful because it provides a spectrum of the planet. Usually both SDI techniques are combined with ADI into sADI to make use of both diversities at the same time. The combined technique of sADI has allowed us to reach the deepest contrasts ever observed (Vigan et al., 2015).

Spectral resolving powers of the order of a few thousand can distinguish between the molecular bands and spectral lines of the star and planet due to the intrinsic difference of their sources (Barman et al., 2015; Hoeijmakers et al., 2018a; Konopacky et al., 2013). An example of the spectral differences at various spectral resolutions of a solar-like star and a giant planet are shown in Figure 1.6. Spectral filters tuned to the host star can be used to remove the starlight while leaving the exoplanet's spectrum largely undisturbed. After removing the starlight a matched-filter is used to combine the various spectral lines of the planet across the spectral range to increase the signal-to-noise. This technique has been used in the Near-Infrared to search for the signatures of different molecules and therefore was coined as Molecule Mapping (Hoeijmakers et al., 2018a). A distinct
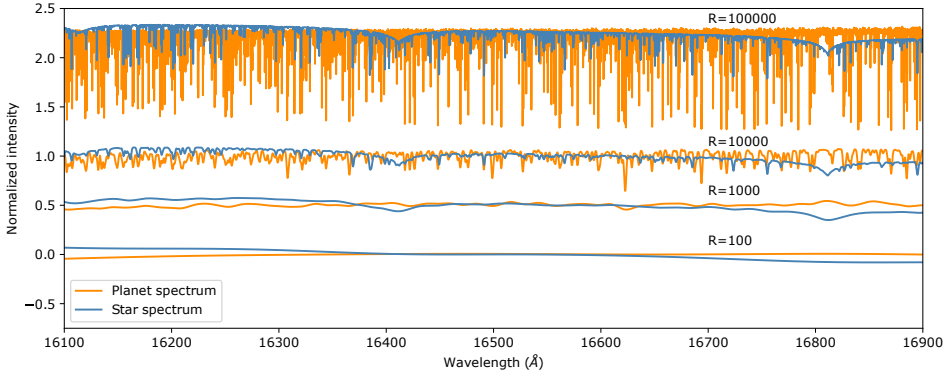
Figure 1.6:   The spectrum of a solar-like star modelled with a 6000 K
PHOENIX model and a spectrum of a giant planet modelled by a 1200 K
BTSettl model. The resolving power changes by one order of magnitude
between the different spectra, going from R=100000 to R=100. The spectra
are shifted for ease of viewing. As the spectral resolving power decreases,
it becomes more difficult to discriminate the planetary spectrum from the
stellar spectrum.

advantage of this technique is that it is not limited by speckle noise, which
hampers the other post-processing techniques.

   An even higher spectral resolving power that is of the order of tens of
thousands to a hundred thousand resolves individual spectral lines. This
increases the capability to discriminate between the planet and stellar fea-
tures. Due to the high resolving power small Doppler shifts on the order of
a few km/s will also become visible. The dynamics of the orbital motion
can then be used as an additional difference to disentangle the planet from
the star (Charbonneau et al., 1999; Snellen et al., 2010). The orbital dif-
ference, without spatially resolving the companion, has been successfully
applied to study several hot giant gas planets, in which many atomic and
molecular species like water, CO (Birkby et al., 2013; Brogi et al., 2014,
2013) and even gaseous iron have been found (Hoeijmakers et al., 2018b).
Even the spin rate and atmospheric dynamics of planetary atmospheres can
be measured by carefully analysing the line profiles (Snellen et al., 2010).
Because the signal-to-noise ratio grows as $\sqrt{R}$ for unresolved lines, it helps
to increase the spectral resolution (Sparks & Ford, 2002). The downside is
that for a fixed detector size the spectral range or the field of view will be
severly limited.

1.2   Thesis outline

The goal of this thesis is to explore the potential of high-resolution integral-field spectroscopy behind a high-contrast imaging instrument for the detection and characterization of exoplanets. The work presented in this thesis can be divided into three parts, the first one focused on coupling a high-contrast imager with a high-resolution spectrograph (R≈100000). The second part shows the scientific gain of integral-field spectroscopy in the visible for high-contrast imaging. And the last part is about a novel way to do spectroscopy with applications for astronomy and Earth observations.

Chapter 2 and 3: The Leiden EXoplanet Instrument(LEXI)
These two chapters present the design, development and on-sky results of the Leiden EXoplanet Instrument (LEXI) a bench-mounted visitor instrument for the 4.2m William Herschel Telescope at La Palma. LEXI was built as a test bed for high-contrast imaging and integral-field spectroscopy. Several different approaches to AO-fed spectroscopy have been tested with LEXI. Our results show that XAO systems are well suited for single-mode fiber spectroscopy. LEXI has also been used to test several wavefront sensing concepts such as the generalised Optical Differentiation Wavefront Sensor (g-ODWFS) (Haffert (2016), Haffert et. al. in prep.), the Coronagraphic Modal Wavefront Sensor (Wilby et al., 2016, 2017) and more recently the Three Wave Shearing Interferometer (TWSI) (Por et al. in prep.).

Chapter 4 and 5: SCAR
These two chapters present the Single-mode Complex Amplitude Refiner (SCAR) coronagraph. SCAR is a promising new coronagraph that makes use of the mode-filtering capabilities of single-mode fibers. This allows us to design and create coronagraphs with higher planet throughput that can search closer to the star. In chapter 5 we present the concept, designs and performance estimates where we show that SCAR enables coronagraphs with inner-working angles close to the diffraction limit. In chapter 6 we experimentally demonstrate the nulling capabilities of SCAR for two differently designs in the lab where we reached a 10^{-4} contrast at 1 λ/D.

Chapter 6: Imaging a forming multi-planet system
This chapter presents the results of High-Resolution Spectral Differential Imaging applied to the system PDS 70 that was observed by MUSE during the commissioning of its new narrow-field mode. MUSE is a medium-

resolution integral-field unit that spans the wavelength range from 0.465μm to 0.93μm at an average resolving power of $R = \lambda/\Delta\lambda = 3000$. The instrument is fed by the LTAO system on UT4 of the VLTs and can reach a spatial resolution of roughly 60 milliarcseconds in good seeing conditions. The combination of the spectral resolving power and the AO performance made it possible to detect two accreting proto-planets in the transition disk around PDS 70. Our observations show that adaptive-optics-assisted, medium-resolution, integral-field spectroscopy with MUSE targeting accretion signatures is a powerful way to trace ongoing planet formation in transitional disks at different stages of their evolution. This was also the first time that a planet has been discovered with an LTAO system, which is very interesting as LTAO can reach a better performance on fainter targets than comparable SCAO systems.

Chapter 7: Novel spectroscopic instrumentation

This chapter presents a novel spectrograph concept based on Volume Bragg Gratings (VBG) that is able to achieve high spectral resolution over a large wavelength range for a large field of view without the need for very large detectors. This is achieved by creating specialized spectral filters with highly multiplexed VBGs (HMBG) that are sensitive to a molecular species of choice. The HMBG condenses the full spectrum into a small, multiplexed spectrum with the size of a single spectral line thereby enabling a large reduction of the required detector real estate per spatial pixel. The chapter presents the concept and a few case studies.

1.3   Outlook

Medium to high-resolution spectroscopy will be a powerful addition to the current and future generation of high-contrast imaging instruments as is demonstrated by the discovery of the second planet in the PDS 70 system (Chapter 6). Our solution to add this capability is to couple high-contrast imaging instruments to spectrographs with single-mode fibers, because they can reduce the complexity of the spectrograph (Chapters 2 and 3) while also enabling improved coronagraph designs with smaller inner-working angles and higher throughput as we have demonstrated with SCAR (Chapters 4 and 5). The success of high-resolution spectroscopy lies in its capability to separate the continuum effects, such as speckle noise, from spectral line features. This does not have to be done in post-processing but can also be done

optically (Chapter 7), and therefore we can reduce the number of required detector pixels per spatial point. With the multiplexed Bragg gratings we can apply the same technique to much larger fields of view and bypass the field-of-view limitation of high-resolution integral-field spectroscopy.

Medium to high-resolution integral-field spectroscopy is likely to be the ideal observing technique to search for accretion signatures from proto-planets. The current standard is to search for Hα emission with Simultaneous Differential Imaging, effectively resulting in resolving powers on the order of $10 - 100$. Signatures such as Hα are intrinsically narrowband, therefore increasing the spectral resolving power of our observations increases the signal-to-noise ratio as long as the line is not resolved. Adding the capability to observe these signatures at much higher resolving power $R = 5000 - 10000$ will increase the signal-to-noise ratio by a factor 10-100 almost for free. MUSE at the VLT does have the capability of integral-field spectroscopy but it was not designed for high-contrast imaging, and therefore lacks the capability for starlight suppression. Development of high-resolution integral-field units for extreme adaptive optics systems will allow us to take the next step in the search and characterization of proto-planets, where we will be able to not only find such planets more efficiently but also can study the process of accretion in detail.

Currently MUSE provides an exciting opportunity to study the time variability of accretion signals from short to long timescales. Such observations will set strong constraints on planet growth and evolution during the earlier stages. In addition due to the unique broad spectral coverage of MUSE, we can observe other accretion tracers such as Hβ at 4861Å, OI at 8446Å, and the CaII triplet at 8498Å, 8542Å, and 8662Å. Together with Hα, the detection of any these tracers will put constraints on the temperature, density and shock velocity at the interface between the planet and the accretion flow.

This work at medium resolution lays down the foundation for visible-light high-resolution integral-field units and high-contrast imaging for the detection of reflected light from cold and old exoplanets, like Earth, and biosignatures such as the O_2 band with the Extremely Large Telescopes (ELT). High-resolution spectroscopy for exoplanets is a photon-starved observing technique. The detection limits are therefore set by the amount of light that we can collect from the star and the planet. Proxima Centauri b could be characterized with the current telescopes but almost a hundred nights spread over three years are necessary to guarantee a detection (Lovis et al., 2017). The effective observing time can be drastically lowered

by using one of the ELTs. ELTs come with two advantages, the first being
the larger collecting area, and the second is the increased spatial resolu-
tion. With an ELT the detection of Proxima Centauri b can obtained in
a single night instead of the hundred nights of VLT time (Snellen et al.,
2015). With the addition of high-resolution integral-field units to extreme
adaptive optics systems at ELTs, we will start to study older, potentially
habitable planets, and thus address humanity's ultimate question: Are we
alone?

Bibliography

Aime, C., & Soummer, R. 2004, ApJ, 612, L85

Andrews, S. M., Rosenfeld, K. A., Kraus, A. L., & Wilner, D. J. 2013, ApJ, 771,
    129

Aoyama, Y., Ikoma, M., & Tanigawa, T. 2018, ApJ, 866, 84

Armitage, P. J., & Belmonte, J. A. 2018, A Brief Overview of Planet Formation
    (Cham: Springer International Publishing), 2185–2203. `https://doi.org/10.`
    `1007/978-3-319-55333-7_135`

Babcock, H. W. 1953, PASP, 65, 229

Baraffe, I., Chabrier, G., Barman, T. S., Allard, F., & Hauschildt, P. H. 2003,
    A&A, 402, 701

Barman, T. S., Konopacky, Q. M., Macintosh, B., & Marois, C. 2015, ApJ, 804,
    61

Benz, W., Ida, S., Alibert, Y., Lin, D., & Mordasini, C. 2014, in Protostars and
    Planets VI, ed. H. Beuther, R. S. Klessen, C. P. Dullemond, & T. Henning, 691

Beuzit, J. L., Vigan, A., Mouillet, D., et al. 2019, arXiv e-prints, arXiv:1902.04080

Biller, B. A., Close, L. M., Masciadri, E., et al. 2007, ApJS, 173, 143

Birkby, J. L., de Kok, R. J., Brogi, M., et al. 2013, MNRAS, 436, L35

Bonaccini Calia, D., Feng, Y., Hackenberg, W., et al. 2010, The Messenger, 139,
    12

Borucki, W. J., Koch, D., Basri, G., et al. 2010, Science, 327, 977

Boss, A. P. 1997, Science, 276, 1836

Bowler, B. P., Liu, M. C., Shkolnik, E. L., & Tamura, M. 2015, ApJS, 216, 7

Brogi, M., de Kok, R. J., Birkby, J. L., Schwarz, H., & Snellen, I. A. G. 2014,
    A&A, 565, A124

Brogi, M., Snellen, I. A. G., de Kok, R. J., et al. 2013, ApJ, 767, 27

Burrows, A., Sudarsky, D., & Hubeny, I. 2004, ApJ, 609, 407

Butler, R. P., Marcy, G. W., Williams, E., Hauser, H., & Shirts, P. 1997, ApJ,
    474, L115

Charbonneau, D., Noyes, R. W., Korzennik, S. G., et al. 1999, ApJ, 522, L145

Chauvin, G., Lagrange, A. M., Dumas, C., et al. 2005, A&A, 438, L25

Chiang, E., & Youdin, A. N. 2010, Annual Review of Earth and Planetary Sciences,
    38, 493

Close, L. M., Follette, K. B., Males, J. R., et al. 2014, ApJ, 781, L30

Codona, J. L., Kenworthy, M. A., Hinz, P. M., Angel, J. R. P., & Woolf, N. J. 2006, in Society of Photo-Optical Instrumentation Engineers (SPIE) Conference Series, Vol. 6269, 62691N

Crockett, C. J., Mahmud, N. I., Prato, L., et al. 2012, ApJ, 761, 164

Dodson-Robinson, S. E., & Salyk, C. 2011, ApJ, 738, 131

Foo, G., Palacios, D. M., & Swartzland er, Grover A., J. 2005, Optics Letters, 30, 3308

Foy, R., & Labeyrie, A. 1985, A&A, 152, L29

Fried, D. L. 1966, Journal of the Optical Society of America (1917-1983), 56, 1372

Fugate, R. Q., Fried, D. L., Ameer, G. A., et al. 1991, Nature, 353, 144

Gaudi, B. S., Stassun, K. G., Collins, K. A., et al. 2017, Nature, 546, 514

Gillon, M., Triaud, A. H. M. J., Demory, B.-O., et al. 2017, Nature, 542, 456

Greenwood, D. P. 1977, Journal of the Optical Society of America (1917-1983), 67, 390

Guyon, O. 2003, A&A, 404, 379

Haffert, S. Y. 2016, Optics Express, 24, 18986

Hennebelle, P., & Chabrier, G. 2008, ApJ, 684, 395, doi: 10.1086/589916

Henry, G. W., Marcy, G. W., Butler, R. P., & Vogt, S. S. 2000, ApJ, 529, L41

Hoeijmakers, H. J., Schwarz, H., Snellen, I. A. G., et al. 2018a, A&A, 617, A144

Hoeijmakers, H. J., Ehrenreich, D., Heng, K., et al. 2018b, Nature, 560, 453

Hubin, N., Arsenault, R., Conzelmann, R., et al. 2005, Comptes Rendus Physique, 6, 1099

Jovanovic, N., Martinache, F., Guyon, O., et al. 2015, PASP, 127, 890

Jovanovic, N., Absil, O., Baudoz, P., et al. 2018, in Society of Photo-Optical Instrumentation Engineers (SPIE) Conference Series, Vol. 10703, Adaptive Optics Systems VI, 107031U

Kasdin, N. J., Vanderbei, R. J., Spergel, D. N., & Littman, M. G. 2003, ApJ, 582, 1147

Kley, W. 2017, arXiv e-prints, arXiv:1707.07148

Konopacky, Q. M., Barman, T. S., Macintosh, B. A., & Marois, C. 2013, Science, 339, 1398

Lee, C.-H. 2017, Research Notes of the AAS, 1, 41

Lenzen, R., Hartung, M., Brandner, W., et al. 2003, in Proc. SPIE, Vol. 4841, Instrument Design and Performance for Optical/Infrared Ground-based Telescopes, ed. M. Iye & A. F. M. Moorwood, 944–952

Lovis, C., Snellen, I., Mouillet, D., et al. 2017, A&A, 599, A16

Lyot, B. 1939, MNRAS, 99, 580

Macintosh, B., Graham, J. R., Ingraham, P., et al. 2014, Proceedings of the National Academy of Science, 111, 12661

Madec, P. Y., Arsenault, R., Kuntschner, H., et al. 2018, in Society of Photo-Optical Instrumentation Engineers (SPIE) Conference Series, Vol. 10703, Adaptive Optics Systems VI, 1070302

Maire, A. L., Skemer, A. J., Hinz, P. M., et al. 2015, A&A, 576, A133

Marcy, G. W., & Butler, R. P. 1996, ApJ, 464, L147

Marleau, G.-D., Klahr, H., Kuiper, R., & Mordasini, C. 2017, ApJ, 836, 221

Marois, C., Doyon, R., Nadeau, D., et al. 2005, PASP, 117, 745

Marois, C., Lafrenière, D., Doyon, R., Macintosh, B., & Nadeau, D. 2006, ApJ, 641, 556

Marois, C., Macintosh, B., Barman, T., et al. 2008, Science, 322, 1348

Marois, C., Zuckerman, B., Konopacky, Q. M., Macintosh, B., & Barman, T. 2010, Nature, 468, 1080

Martinez, P., Kasper, M., Costille, A., et al. 2013, A&A, 554, A41

Masuda, K. 2014, ApJ, 783, 53

Mayor, M., & Queloz, D. 1995, Nature, 378, 355

McKee, C. F., & Ostriker, E. C. 2007, ARA&A, 45, 565

Morbidelli, A., & Raymond, S. N. 2016, Journal of Geophysical Research (Planets), 121, 1962

Mulders, G. D., Pascucci, I., Apai, D., & Ciesla, F. J. 2018, AJ, 156, 24

Nelson, R. P., Papaloizou, J. C. B., Masset, F., & Kley, W. 2000, Monthly Notices of the Royal Astronomical Society, 318, 18

Nero, D., & Bjorkman, J. E. 2009, ApJ, 702, L163

Otten, G. P. P. L., Snik, F., Kenworthy, M. A., et al. 2017, ApJ, 834, 175

Pascucci, I., Testi, L., Herczeg, G. J., et al. 2016, ApJ, 831, 125

Petigura, E. A., Howard, A. W., & Marcy, G. W. 2013a, Proceedings of the National Academy of Science, 110, 19273

Petigura, E. A., Marcy, G. W., & Howard, A. W. 2013b, ApJ, 770, 69

Petit dit de la Roche, D. J. M., Hoeijmakers, H. J., & Snellen, I. A. G. 2018, A&A, 616, A146

Pollack, J. B., Hubickyj, O., Bodenheimer, P., et al. 1996, Icarus, 124, 62

Racine, R., Walker, G. A. H., Nadeau, D., Doyon, R., & Marois, C. 1999, PASP, 111, 587

Rameau, J., Chauvin, G., Lagrange, A. M., et al. 2013, A&A, 553, A60

Rasio, F. A., Shapiro, S. L., & Teukolsky, S. A. 1992, Astronomy and Astrophysics, 256, L35

Rouan, D., Riaud, P., Boccaletti, A., Clénet, Y., & Labeyrie, A. 2000, PASP, 112, 1479

Rousset, G., Lacombe, F., Puget, P., et al. 2003, in Proc. SPIE, Vol. 4839, Adaptive Optical System Technologies II, ed. P. L. Wizinowich & D. Bonaccini, 140–149

Ruane, G., Mawet, D., Jewell, J., & Shaklan, S. 2017, in Society of Photo-Optical Instrumentation Engineers (SPIE) Conference Series, Vol. 10400, Society of Photo-Optical Instrumentation Engineers (SPIE) Conference Series, 104000J

Ruane, G., Ngo, H., Mawet, D., et al. 2019, AJ, 157, 118

Schneider, G., & Silverstone, M. D. 2003, in Proc. SPIE, Vol. 4860, High-Contrast Imaging for Exo-Planet Detection., ed. A. B. Schultz, 1–9

Skemer, A. J., Marley, M. S., Hinz, P. M., et al. 2014, ApJ, 792, 17

Smith, B. A., & Terrile, R. J. 1984, Science, 226, 1421

Snellen, I., de Kok, R., Birkby, J. L., et al. 2015, A&A, 576, A59

Snellen, I. A. G., de Kok, R. J., de Mooij, E. J. W., & Albrecht, S. 2010, Nature, 465, 1049

Snik, F., Otten, G., Kenworthy, M., et al. 2012, in Society of Photo-Optical Instrumentation Engineers (SPIE) Conference Series, Vol. 8450, Modern Technologies in Space- and Ground-based Telescopes and Instrumentation II, 84500M

Soummer, R. 2005, ApJ, 618, L161

Soummer, R., Aime, C., & Falloon, P. E. 2003, A&A, 397, 1161

Sparks, W. B., & Ford, H. C. 2002, ApJ, 578, 543

Tallon, M., & Foy, R. 1990, A&A, 235, 549

Tavani, M., & Brookshaw, L. 1992, Nature, 356, 320

Thatte, N., Abuter, R., Tecza, M., et al. 2007, MNRAS, 378, 1229

Traub, W. A., & Oppenheimer, B. R. 2010, Direct Imaging of Exoplanets (University of Arizona Press), 111–156

van Eyken, J. C., Ciardi, D. R., von Braun, K., et al. 2012, ApJ, 755, 42

Vigan, A., Gry, C., Salter, G., et al. 2015, MNRAS, 454, 129

Vorobyov, E. I. 2013, A&A, 552, A129

Wilby, M. J., Keller, C. U., Haffert, S., et al. 2016, in Society of Photo-Optical Instrumentation Engineers (SPIE) Conference Series, Vol. 9909, Adaptive Optics Systems V, 990921

Wilby, M. J., Keller, C. U., Snik, F., Korkiakoski, V., & Pietrow, A. G. M. 2017, A&A, 597, A112

Wizinowich, P., Acton, D. S., Shelton, C., et al. 2000, PASP, 112, 315

Wolszczan, A., & Frail, D. A. 1992, Nature, 355, 145

Yu, L., Winn, J. N., Gillon, M., et al. 2015, ApJ, 812, 48

Zhu, Z. 2015, ApJ, 799, 16